Nano Research
2022, 15(6): 5425–5434

ISSN 1998-0124 CN 11-5974/O4
https://doi.org/10.1007/s12274-022-4125-9

Research Article

Fully self-powered instantaneous wireless liquid level sensor system based on triboelectric nanogenerator

Liangquan Xu[1], Yuzhi Tang[1], Chi Zhang[2,3], Fuhai Liu[1,4], Jinkai Chen[1], Weipeng Xuan[1] (✉), Hao Jin[2,3], Zhi Ye[2,3], Zhen Cao[2,3], Yubo Li[2,3], Xiaozi Wang[2,3], Shurong Dong[2,3], and Jikui Luo[2,3] (✉)

[1] *Ministry of Education Key Laboratory of RF Circuits and Systems, College of Electronics & Information Hangzhou Dianzi University, Hangzhou 310018, China*
[2] *College of Information Science and Electronic Engineering, Zhejiang University, Hangzhou 310027, China*
[3] *International Joint Innovation Center, Zhejiang University, Haining 314400, China*
[4] *Special Equipment College, Hangzhou Vocational & Technical College, Hangzhou 310018, China*

Received: 8 November 2021 / **Revised:** 29 December 2021 / **Accepted:** 30 December 2021

ABSTRACT

Self-powered sensors are highly sought for wireless sensing applications in space exploration, industries, and environmental monitoring, etc. However, most current self-powered sensor technologies are based on the multiple energy conversion routine: energy collection, rectification, energy storage, and power management before it can be used for sensor systems, leading to exceptionally low energy utilization efficiency and very short periods of wireless sensing operation with majority of information lost. Here, we propose a triboelectric nanogenerator (TENG) based fully self-powered instantaneous and real-time wireless sensor system which does not contain electronic devices and microchips, but the passive components only. An innovative cylindrical capacitive-type liquid level sensor is also proposed and is then integrated into the wireless sensor system for monitoring liquid levels or identifying substance of the liquids. This sensor system can convert pulsed voltage output of the TENG into sinusoidal signal with a resonant frequency containing the sensing information and is transmitted to the receiver in distance in real-time. The maximum transmission distance of the sensor system could reach 1.5 m for a 10 cm diameter magnetic-core coil pair. The wireless sensor system exhibited excellent stability and excellent linearity with a sensitivity of 4.63 kHz/cm, and demonstrated its great application potential for the self-powered liquid level monitoring.

KEYWORDS

triboelectric nanogenerator, self-powered sensor, liquid level sensing, wireless and chipless sensor

1 Introduction

With the development of modern society and the increasing frequency of extreme climate nowadays [1–3], we not only need the green and sustainable development [4–6], but also have to prevent natural disasters and accidents [7]. Continuous monitoring of liquid levels plays an important role in preventing flood/draught and industrial incidents to ensure the safety of lives and continuous production. Microsensors have been widely utilized to monitor liquid levels in various fields, such as in cars for the petrol level, in liquid propanol gas shipping vessels for the liquid propanol level, in machineries for the coolants and lubricant oils, etc. [8–11]. For nuclear power plants, it is essential to monitor the real-time coolant level of the nuclear reactor to ensure its safe and efficient operation [12, 13]. When the coolant level is not within the specified range, an alert would be raised so that necessary measures can be taken to ensure safe operation. In the environmental monitoring field, liquid level sensor is used to monitor the real-time water level of a reservoir to ensure the efficient and safe operation of the reservoir and hydropower generators. This is especially important for the frequent extreme climate faced nowadays.

At present, electronic sensors are generally used to monitor liquid levels. It is generally required for these sensors to work wirelessly, especially for the monitoring in remote and harsh environments. Traditional wireless liquid level sensors normally contain many electronic devices and microelectronic modules, including analog-digital (AD) module, signal processing module, transmission module, energy management module, registers, and most importantly the power source [14–20]. Electric powers are needed to operate the sensors, electronic modules, and wireless transmitter, and batteries are still the choice of power sources for wireless sensor networks. In order to make the wireless sensor networks work continuously, periodical replacement of batteries and maintenance are essential. These make the wireless sensor systems complicated, resource-intensive, and expensive, but also produce a large number of waste batteries which will pollute the environment; thus, it is not in line with the current trend of green and sustainable development.

There is a new development trend for the wireless sensor systems, i.e., the self-powered wireless sensor systems that are able to harvest energy from the environments and convert it into electricity to run the whole sensor systems without needing additional power sources [21–23]. The commonly used devices to

Address correspondence to Weipeng Xuan, xuanweipeng@hdu.edu.cn; Jikui Luo, jackluo@zju.edu.cn

harvest energy are the solar cells, geothermal generators, piezoelectric nanogenerators (PENG), and triboelectric nanogenerators (TENG), etc. [24–28]. The solar cells and geothermal generators strongly rely on the environments they are present, thus limit their applications to special places, while PENG have small output power, not sufficient for most of the applications. On the other hand, TENGs have large power outputs and high energy conversion efficiency, and have been utilized for many sensing applications [29–32]. However, currently this type of TENG- or PENG-based self-powered wireless sensor systems involves multiple energy conversion steps: energy harvesting, rectification, storage, and power regulation to supply the sensor systems, making the final energy utilization efficiency exceptionally low [33–35]. It normally requires long duration to collect sufficient energy to power the system for sensing and wireless transmission for very short time, typically in a few milli-seconds (ms) to tens of ms, and they are not instantaneous and real-time sensing so that most of the information are lost. Because the real-time monitoring of liquid level is extremely important for the safety of people and production, it is essential for continuous and instantaneous monitoring of liquid level, with the latter particularly important for disaster and accident prevention and management such as flood and ship damage, etc.

The latest development for self-powered wireless sensor systems is to utilize TENG to collect energy and directly convert it into oscillating signals with encoded sensing information and transmit it wirelessly to the receiver, with no or very little electronic devices involved [36, 37]. By connecting a TENG with an inductor coil, it formed an LC circuit that can directly convert pulse output of the TENG into resonant signal, and the frequency of resonant signal can be controlled by changing the capacitance value of the LC circuit; this was utilized to fabricate a contactless keyboard with different tunes [38]. This novel concept of TENG-driven LC oscillating circuit laid the foundation for further development of various fully self-powered wireless sensors. To increase the signal amplitude and distance of transmission, a synchronized microswitch was then introduced between TENG and LC circuit, and an additional identity (ID) capacitance was used to form the LC circuit with a fixed resonant frequency with no interferences from the TENG operation that greatly increased transmission signal; by coupling the oscillation signal with a laser diode, wireless sensing up to 4 m was realized [39]. A magnetic resonant coupling theory was then developed for TENG to transmit energy wirelessly using coupled inductor coils, with the transmission efficiency as high as 78% for a distance of 5 cm; and magnetic resonance-couple wireless sensors for force and pressure were obtained with self-identity [40]. Inspired by these novel concepts, various fully-self powered magnetic resonance coupled wireless TENG sensors were developed for humidity sensing, traffic monitoring and control, metallic component detection for product line management, tire pressure, and speed monitoring, etc. [41–45]. The TENG-based fully self-powered sensor systems are able to perform sensing as well as transmitting signal wirelessly instantaneously, either by light or by radio frequency (RF) electromagnetic waves [40–42]. For the RF wireless sensing systems, it was based on the magnetic resonance coupled wireless transmission, and the TENG devices acted as both the power source as well as the force (pressure) sensor. Other types of sensors such as humidity, temperature sensor can be integrated into the LC resonance circuit of the system, so that any variation of the sensors could be encoded into the resonant signal for the self-powered wireless sensing. Since there is no rectification, energy storage and power regulation processes involved, this type of sensor systems has very high energy utilization efficiency, and has the instantaneous and real-time sensing, and wireless transmission capability, yet has no additional electronic devices and microchips, but the passive resistors, capacitors, and inductors.

This work reports a further development of the TENG-based instantaneous, wireless and chipless liquid level sensor system. A cylindrical type of liquid level sensor is developed and integrated into the TENG-based wireless sensor system. By utilizing a small ferric magnetic core for the transmission coils, a fully self-powered wireless liquid level sensor system with much reduced dimensions of sensing system and longer transmission distance is obtained. Depending on the application scenarios, the sensor system is capable of detecting liquid level variation from millimeter to tens of centimeters, with a high sensitivity of 4.626 kHz/cm. The sensor system is also capable of identifying substances of the liquids.

2 Results and discussion

2.1 Working principle of the wireless liquid level sensor system

In this section, the configuration and circuit model of the TENG-based self-powered instantaneous wireless liquid level sensor system are explained in detail. Figure 1(a) shows the schematic configuration of the wireless sensor system. The transmitter consists of a TENG integrated with a synchronized micro-mechanical switch, an LC resonant circuit. The capacitance C is the total capacitance of the capacitive liquid level sensor and the base capacitor that are connected in parallel. The base capacitor C_{ID} has a constant capacitance and is to stabilize the signal and adjust the sensitivity of the sensor as will be discussed later. The receiving terminal is composed of an LC circuit in series connection which will have the same resonant frequency as that of the transmitter, so that a magnetic resonance coupling can be established between the two terminals. When an external force such as vibration or rolling activates/triggers the TENG, it generates a pulsed voltage (energy) output, which is injected into the LC resonant circuit to produce an attenuation oscillating signal with a fixed resonant frequency. The oscillating signal is transmitted wirelessly to the receiving terminal via the magnetic resonance coupling. The receiver circuit processes and analyzes the received signal, and displays the results, or raises warning signal if necessary.

The equivalent circuit diagram of the sensor system is shown in Fig. 1(b). V_{TENG} and C_{TENG} are the pulsed voltage output and equivalent capacitance of the TENG [46]. The switch is a synchronous micro-mechanical switch, which closes when two triboplates of the TENG separate from each other to the maximum distance and opens for all other situations. A diode (1N4007) is connected in parallel with the microswitch, which enables electrons to flow back to the metal electrode when the synchronized microswitch is used in the TENG. The typical output signals of the TENG with/without a microswitch integrated are shown in Fig. 1(c). The output of the TENG with a microswitch can reach a peak voltage of over 2,200 V, much larger than that (typically ~ 1,500 V) without the microswitch integrated. The negative voltage corresponds to the voltage generated by the charges flowing back to the metal electrode through the diode. The much enhanced voltage output of the TENG with the microswitch is because the much reduced discharging time as explained in detail in our previous paper [39].

C_S is the capacitance of the liquid level sensor. It connects in parallel with the base capacitor C_{ID}. A pair of magnetic core coils is used which makes the sensor system with much smaller dimensions for longer transmission distance [42]. The capacitance C_S is a sensing variable for the liquid level to be monitored. The base capacitor C_{ID} is used to determine the reference frequency of

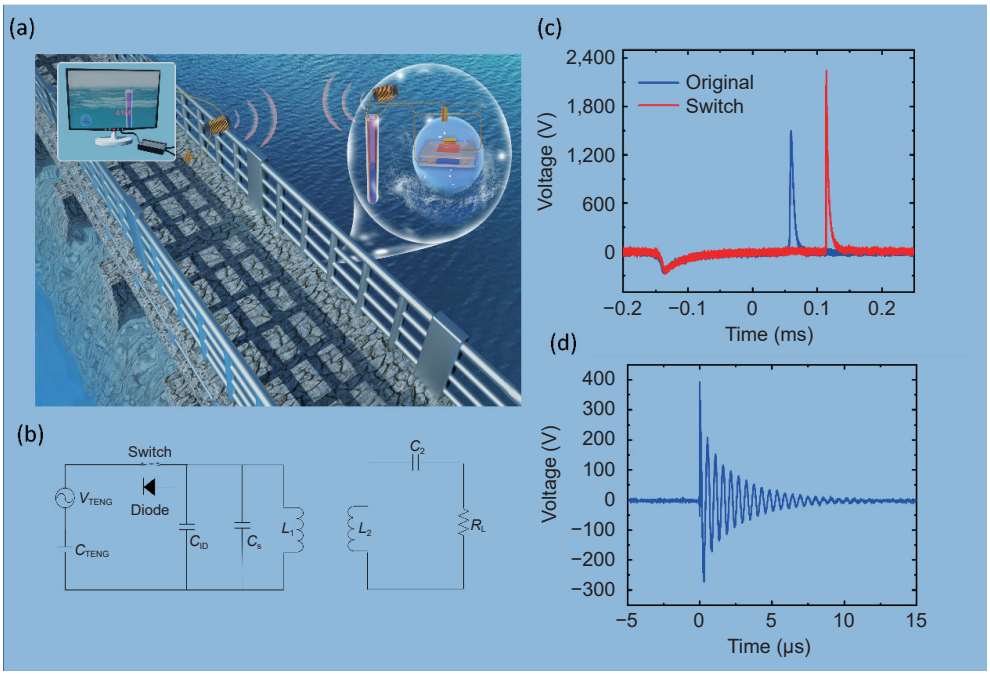

Figure 1 (a) Schematic diagram of the TENG-based self-powered wireless liquid sensor system, (b) the equivalent circuit diagram of the transmitter and receiver, respectively, (c) typical voltage outputs of a TENG integrated with/without a synchronization microswitch, and (d) typical transmitter oscillating signals with a fixed resonant frequency.

the oscillating signal and makes the signal more stable as will be discussed later. The base resonant frequency could also be utilized as the ID of the sensor system. The L_2 and C_2 are the magnetic core coil and tuning capacitor of the receiver, and they form an oscillating circuit and is utilized to receive the signal from the transmitter via magnetic resonance coupling wirelessly. The typical transmitted signal is shown in Fig. 1(d). As it can be seen that a single pulsed voltage output of the TENG can be converted into an attenuation oscillating transmission signal. The maximum signal amplitude V_{PP} is over 400 V with a fixed resonant frequency. Correspondingly, the received signal normally is an enveloped attenuation sinusoidal signal with the same resonant frequency as that of the transmitter, and the maximum signal amplitude is reduced to V_{PP} ~ 80 V for a transmission distance of 20 cm due to the consumption of the limited (pulsed) energy and wireless transmission. Details will be discussed later.

2.2 High performance of TENG with surface plasma treatment

For the demonstration of self-powered liquid level sensing using TENG, the contact-separation mode TENG was adopted in this work. The schematic diagram of the contact-separation mode TENG is shown in Fig. 2(a). The contact-separation mode TENG can be used to harvest various forms of kinetic energy. Our previous works have proved that TENGs with stronger energy collection capability are more conducive to wireless sensing system [40]. Although TENGs have superior performance as compared to other types of energy harvesting devices, the performances of TENGs can be further enhanced by using tribo-material pairs with large electronic affinity difference. Our previous work has shown that nylon-66 (PA66) and fluorinated ethylene propylene (FEP) is an excellent material combination for the fabrication of high performance of TENGs [42]. They were used as the tribo-plates for the TENG in this work, with the PA66 as the positive triboelectric material and FEP polymer as the negative triboelectric material. The thickness of both the tribo-membranes was 100 μm, and the active area of them was 5 cm × 5 cm. Adhesive copper foils with a thickness of 100 μm was used as the electrodes for both the tribo-plates, and they were adhered on backs of both the tribo-membranes. To further promote the performance of the PA66/FEP TENG, an oxygen plasma treatment was utilized to activate the friction surface of the PA66 to increase the surface charge density [47]. The oxygen plasma treatment makes PA66 tribomaterials with more tribo-positive property, i.e., easier to lose electrons, thus obtain the TENG with higher performance. A comparison of voltage outputs and surface characterization for TENGs with and without plasma treatment is shown in SI1 in the Electronic Supplementary Material (ESM). As it can be seen from Fig. S1 in the ESM, that the oxygen plasma treatment could greatly increase the output voltage of the TENG. The increase is mainly attributed to the much-increased surface potential after plasma treatment for the PA66 as exhibited by Fig. S1(f) in the ESM measured by Kelvin probe force microscope (KPFM). The two triboplates were then assembled into a contact-separation mode TENG with a maximum spacer of 4 mm using four springs as the supports. A diode (1N4007) was connected between the copper electrodes of the two tribo-plates, which enables electrons to flow to the metal electrode when the synchronized microswitch is open in the TENG during the operation. More information of the TENG fabrication can be found in Methods.

The general operation process of the contact-separation mode TENG is well-known. For clarification, it is explained here as shown in Fig. 2(b). When the two tribo-plates of the TENG is contacted, charges with opposite polarities are induced on the surfaces of PA66 and FEP membranes respectively, through the electrification effect. When the two tribo-plates are separating, the circuit is at the open state. An electrical potential is established between the two triboplates, and it increases with the increase of separation distance of the two triboplates due to the accumulated charges on surfaces of the two tribomaterials that can not flow through the reversely connected diode. When the separation distance of the two triboplates reaches the maximum, the microswitch is closed and electrons from the PA66 plate flow to the FEP plate through the external circuit with a load instantaneously, and a positive pulsed voltage output is generated. When the two tribo-plates are closing, the microswitch is at the open state and electrons from the back electrode of the FEP plate

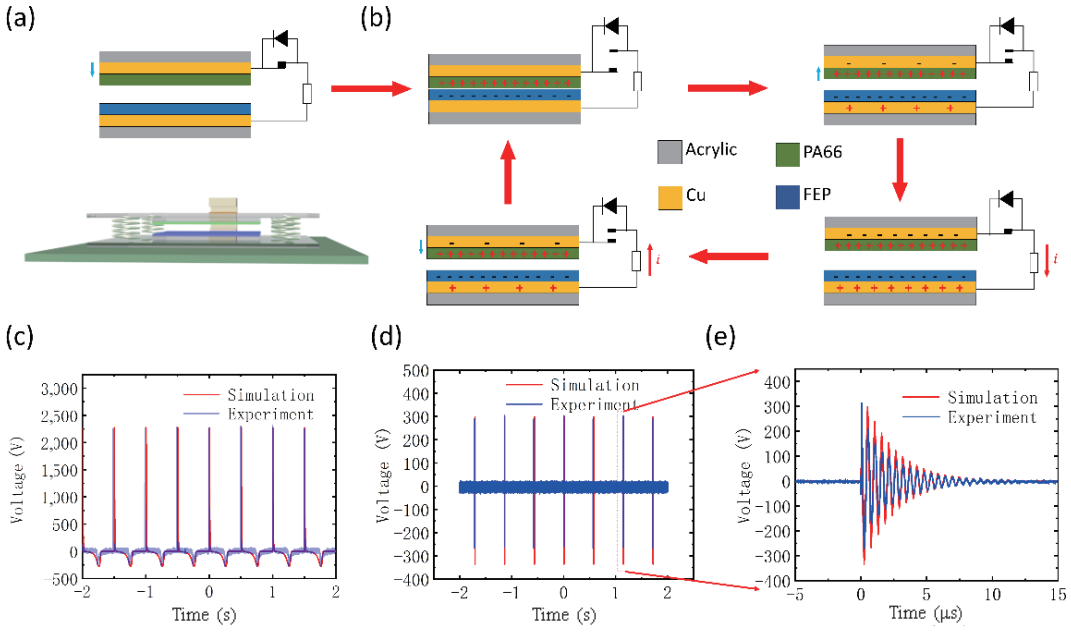

Figure 2 (a) Schematic diagram of TENG fabricated, (b) the working sequences of the TENG. (c) The voltage output of the TENG with an integrated microswitch under a force of 50 N, a frequency of 2 Hz, and a spacer of 4 mm; (d) As TENG works under repeated stimulation, it will produce resonance signals, (e) the resonant signal generated at the transmitter with a maximum V_{PP} of over 400 V. The simulated results for the outputs of the TENG are also shown in (c)–(e) for comparison with the experimental results, showing good agreement between them.

flow to the back electrode of the PA66 plate through the diode to balance charges on the two plates through the electrostatic induction effect, which corresponds to the negative voltage output. When the two tribo-plates are back in contact, all induced charges are neutralized.

Under the condition of an applied force of 50 N and a contact frequency of 2 Hz, the output of the TENG can reach over 2,200 V with a 100 MΩ load as shown in Fig. 2(c), which is close to the threshold voltage of air ionization between the two triboplates. Higher voltage will have more energy output from the TENG, which is beneficiary for the wireless sensor system. For the wireless transmission system, the energy loss in the transmission process is related to the transmission distance, thus the signal with higher energy can have a longer transmission distance.

If the load of Fig. 2(b) is replaced by an LC parallel circuit, the output voltages of the TENG will become a series of attenuating resonant signals, as shown in Figs. 2(d) and 2(e). It can be seen that the maximum peak-to-peak voltage, V_{PP} > 300 V, of the resonance signal is much less than 2,200 V of the TENG output voltage. There are a few reasons responsible for this. Firstly, the impedance of the LC circuit, less than one hundred ohms, is much smaller than the output impedance (~ 20 kΩ) of the TENG with the microswitch as shown in Fig. S1(c) in the ESM. As a result, the coupled voltage from the TENG to the LC resonant circuit is very small even though the microswitch has greatly reduced the output impedance of the TENG as shown in Figs. S1(b) and S1(c) in the ESM, so that the voltage across the LC resonant circuit is small. Secondly, the LC circuit consumes a certain portion of the injected energy from the TENG, and the energy consumption is determined by the quality factor Q of the LC circuit, which normally is relatively small for LC circuit. Also, the energy is distributed to multiple oscillations, not to one single oscillation. The detailed waveform of the LC resonance signal is shown in Fig. 2(e), which is the transmission signal of the TENG-based wireless transmission system. As it can be seen the signal amplitude decays very fast with time, and there are a few tens of oscillation before it becomes almost zero. Based on the circuit parameters, we have conducted signal output simulation for the circuit by using Simulink software. The simulated output of TENG and oscillating signal of the transmitter are shown in Figs. 2(d) and 2(e) for comparison with the experimental ones, showing that the simulated and experimental results are in good agreement. Details of the simulation is shown in SI2 in the ESM.

The typical received oscillating signal by the receiver has a V_{PP} ~ 80 V at a transmission distance of 20 cm, depending on the sensing situations which will be explained later. If the liquid level sensor system is used to monitor water level in a reservoir, then the contact-separation mode TENG can be installed in a box to harvest the energy from the wave-induced movement with a mass loading [48, 49]; if it is used to monitor coolant or machinery lubricant level, then machine vibration can be utilized as the kinetic energy to operate the TENG [50]. Other types of TENGs such as the sliding mode, rolling mode, and rotating mode TENGs, are also suitable for the proposed self-powered wireless sensing application, and will not be repeated here in detail.

2.3 Liquid level sensor design and theoretical analysis

For the demonstration of wireless liquid level sensing, a cylindrical liquid level sensor has been developed. The structure of the liquid level sensor and its fabrication process, and a three-dimensional (3D) model are shown in Fig. 3(a). A tube (here it is glass) with open ends was used as the base of the liquid level sensor. Two copper foils with a width, y, of 20 mm were adhered on the outside of the glass tube along the tube direction as the electrodes for the sensor. The copper electrodes, glass, and the medium inside the glass tube (air and liquid) form a capacitor, and the glass and internal substance are the dielectric medium of the capacitor. In order to prevent the copper electrodes from forming a short circuit when the sensor was immersed in liquid, another hollow glass tube with a slightly larger diameter was placed to cover the copper electrode of the inner tube, and was then filled with a type of waterproof insulating paint to seal the gap between the two glass tubes. The length, h_0, of the glass tube was 100 cm, and the radius, R, of the inner glass tube was 10 mm, and thickness, x_0, of the glass tube wall was 2 mm.

To make the liquid level sensing system used in much broader areas with general implication, theoretical analysis was conducted for the capacitive sensor. A two-dimensional (2D) cross sectional

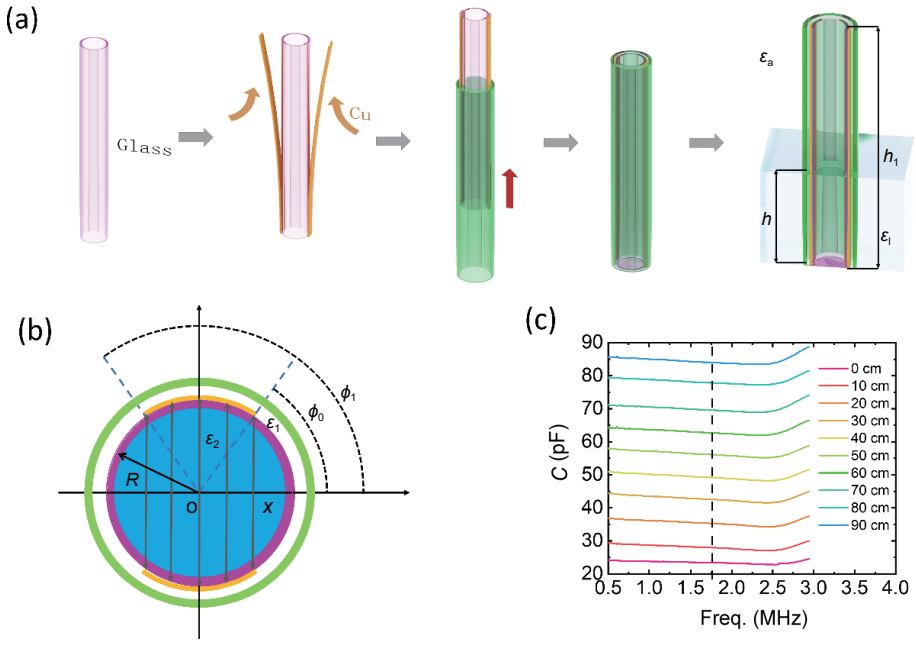

Figure 3 (a) Structure and fabrication process of the liquid level sensor, (b) Cross section of the sensor and the related parameters, (c) dependence of capacitance of the sensor on liquid level height for the sweep frequency range between 0.5 and 3 MHz.

model of the sensor is shown in Fig. 3(b), and the sensor can be considered as the semi-cylindrical capacitor with its capacitance value depending on the liquid level inside the tube. The capacitance of the semi-cylindrical capacitor is a function of the liquid level height, *h*. This function can be expressed as Eq. (1). The detailed derivation of the formula is shown in SI3 in the ESM

$$C_s(h) = \sum_{k=1}^{n} \frac{\varepsilon_0 \frac{ph}{n}}{\frac{2R\sin(\phi_0+\Delta\phi)}{\varepsilon_l} + \frac{2x_0}{\varepsilon_g}} + \sum_{k=1}^{n} \frac{\varepsilon_0 \frac{p(h_0-h)}{n}}{\frac{2R\sin(\phi_0+\Delta\phi)}{\varepsilon_a} + \frac{2x_0}{\varepsilon_g}} + C_{air} \quad (1)$$

where ε_l is the liquid dielectric constant, ε_a is the air dielectric constant, ε_g is the glass dielectric constant, p is the arc length of the electrode patch, h_0 is the total length of the glass tube, R is the inner radius of the cylinder, and φ_0 is the angle from the center of the circle O to the rightmost side of the electrode patch at the coordinates as shown in Fig. 3(b). $\Delta\varphi$ can be expressed by Eq. (2)

$$\Delta\phi = \frac{(\phi_1 - \phi_0)}{n-1} \quad (2)$$

where φ_1 is the angle from the center of the circle O to the leftmost side of the electrode patch. Detailed analysis of the liquid level sensor and equation deduction can be found in SI3 in the ESM.

Knowing the value of C_s, then the resonant frequency of the oscillating signal of the transmitter can be determined by the following Eq. (3)

$$f = \frac{1}{2\pi\sqrt{L_1(C_s + C_{ID} + C_{TENG} + C_{par})}} \quad (3)$$

here C_{par} is the parasitic capacitance of the system. Capacitances of the sensor were measured by an impedance analyzer (Keysight E4990A) at different liquid levels for the frequency range between 500 kHz and 3 MHz, with the results shown in Fig. 3(c). It can be seen that the capacitance value of the sensor increases with the rise of liquid level for a fixed testing frequency, while it remains relatively flat for most of the tested frequencies except when the frequency range exceeds 2.5 MHz, where it increases with frequency rapidly. For the experiments, a fixed testing frequency can be chosen, for instance at 2 MHz, then the sensor can respond well to the liquid level, i.e., it can be used as the capacitive sensor to monitor liquid level. When the liquid level is zero, the capacitance of the sensor is C = 19.5 pF, when the liquid level increases to 90 cm, the capacitance rises to 90.2 pF because the dielectric constant of liquid is larger than that of air. When the liquid level sensor is integrated into the wireless liquid level sensor system, the system will respond to the change of liquid level sensitively, represented by the change of the resonant frequency as well as the signal amplitude as will be discussed below.

Although the liquid level sensor developed is large and is for sensing liquid in large volume such as in a reservoir, the sensing method and theory, and the type of liquid level sensor developed have the general implications, and can be applied to sensing cases requiring macrosensors or microsensors as long as it is a capacitive type of sensors. Thus, the self-powered real-time wireless sensor system can be applied to monitor water level in reservoirs, coolant levels in machineries, and nuclear reactor, etc.

2.4 Response of the wireless sensor to liquid level variation

When the liquid level sensor as the capacitor, C_S, is integrated into the sensing system as shown in Fig. 1(b), it forms the liquid level sensing system. Detailed analysis was conducted for the proposed TENG-based wireless sensor system, it showed that, when the system is at the magnetic resonance state, the received signal composed of two components with a single resonant frequency, ω, and the specific expression is shown by Eq. (4)

$$v(t) = Ae^{-at}(k_1\cos(\omega t) + k_2\sin(\omega t)) - k_3e^{-\tau t} \quad (4)$$

where A, k_1, k_2 and k_3 are the pre-factors of each signal, α and τ are the attenuation factors, and ω is the angular frequency.

The typical signal generated by the transmitter of the sensor system is shown in Fig. 4(a) in comparison with the received signal for a transmission distance of 20 cm. As shown in the fiugre, the two signals have the same resonant frequency, though the amplitudes of the signals are different. Fast Fourier transform (FFT) was applied to analyze the two signals with the spectral

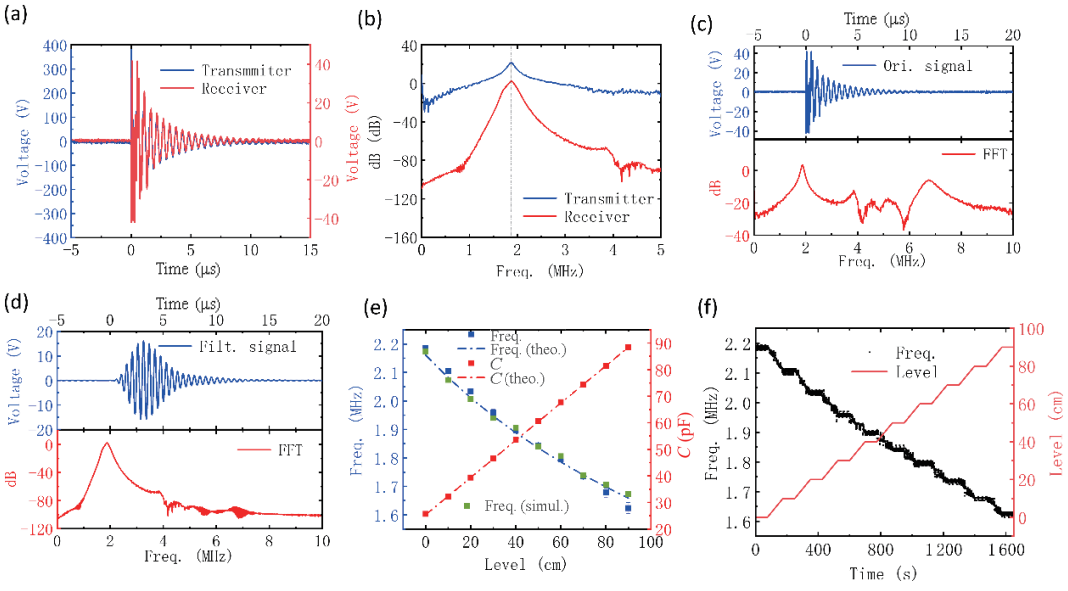

Figure 4 (a) Comparison between the transmitting signal and received one for a transmission distance of 20 cm, (b) FFT spectra comparison between the transmitting and received signals. (c) Received signal and FFT spectrum, (d) received signal and FFT spectrum after filtering, and (e) the capacitance value of the liquid level sensor and the average resonant frequency of the sensor system as a function of water level. Clean tap water was used for the experiments. (f) Level response of the wireless liquid level sensor system to step change of level.

results shown in Fig. 4(b). The resonant frequencies of the transmitted and received signals are the same, about 1.9 MHz, indicating the resonant frequency of the transmitted signal is not affected by the transmission system.

It can be seen from the FFT spectrum of the received signal, there are a few of resonant peaks and noises with the frequencies greater than 3 MHz as shown in Fig. 4(c), which is due to the parasitic resonances, not from the transmitter [40, 41]. The noise and parasitic resonances can be easily removed by using the Chebyshev bandpass filter. The FFT spectrum of the received filtered signal is shown in Fig. 4(d) for comparison. As it can be seen the amplitude of the undesired peaks has become much smaller whereas the resonant peak remains almost unchanged, implying the filtering is effective to remove undesirable signals. After filtering, the received signal becomes a typical envelope shape in the time domain, and it is due to the start of the oscillation of the signal.

When the liquid level varies, the sensor capacitance changes and the resonant frequency of the oscillating signal varies accordingly, which can be detected by the receiver in distance, realizing instantaneous wireless monitoring of the liquid level. With liquid level rising, the resonant frequency shifts to low values due to the increased capacitance of the sensor, and vice versa. Dependence of the sensor capacitance and the resonant frequency of the sensor system on liquid level (clean water) are summarized in Fig. 4(e) by the blue and red colored dots respectively. For the experimental ones, each liquid level is the average value of 50 measurements for more accurate measurements. The capacitance of the sensor varies in the range between 21 and 90 pF when the liquid level is in the range of 0–90 cm and the capacitance of the sensor is linearly correlated to liquid level for the water level range measured with a gradient of 0.7 pF/cm. According to Eq. (4), the oscillating frequency is nonlinearly correlated with liquid level, which varies in the range between 2.19 and 1.62 MHz when the liquid level is in the range of 0–90 cm. It can be seen that the wireless sensor system has good responses to the liquid level variation, and indeed can be utilized to monitor the real-time water level wirelessly. The capacitance of the sensor and resonant frequency of the transmitter were calculated according to the theories discussed above, with the results shown in Fig. 4(e) by red and blue dashed lines respectively. The resonant frequencies were also simulated using the circuit simulation software Simulink (green dots). It can be seen that the curves of the theoretical calculation results, simulated and experimental results are in excellent agreement, indicating the correctness of the above theories and analysis. Detailed circuit and simulation can be found in SI3 in the ESM. Figure 4(f) shows responses of the sensor system to step changes of liquid level, the response of the frequency of the sensor is instantaneous, and mostly limited by the rising speed of the liquid, instead of the sensor system itself. The results demonstrate the excellent stability and repeatability of liquid level sensing and its instantaneous wireless sensing capability.

2.5 Effects of different types of liquids

As shown by Eqs. (1) and (3), the resonant frequency of the sensor system is related to capacitance of the liquid level sensor, whereas the capacitance of the liquid level sensor depends on dielectric constant, ε_l, of the liquid and active area (the relative liquid level). The frequency response of the sensor system to different types of liquids at the same liquid level will be different, because of the different dielectric constants. This allows the sensor system to be used for sensing or identifying the type of liquids in the container. Under the conditions of Table 1, the frequency response of the sensor system to different liquids was investigated with the results shown in Fig. 5(a), all at the same liquid level of h = 40 cm and

Table 1 parameters of the wireless sensor system

Capacitance Cs	Variable
Capacitance C_2	220 pF
Transmission distance, d	20 cm
Diameter of coil 1, D	10 cm
Diameter of coil 2, D	10 cm
Inductance L_1	60 μH
Inductance L_2	60 μH
Load R_L	300 Ω
C_{ID}	30 pF
Coil type	Magnetic core

transmission distance of 1 m. The resonant frequency of the sensor system is around 2.10 MHz when the liquid level is zero for different types of liquids. This is because there is no liquid inside the sensor, hence the resonant frequency is the same. As the liquid level rises, differences in resonant frequency responses to different liquids can be seen clearly, due to the different dielectric constants. Among the three types of liquids, the dielectric constant of clean water is the largest, about 81, so its resonant frequency decreases the fastest from 2.20 to 1.62 MHz due to the fastest increase of capacitance as the liquid level increases from zero to 90 cm, the 95% glycerin has a dielectric constant of about 41, and the resonant frequency of the sensor system drops from 2.20 to 1.70 MHz for the same liquid level change. 75% ethanol has the smallest dielectric constant, about 34.6, and the resonant frequency decreases from 2.20 to 1.72 MHz.

The amplitudes of the received signals corresponding to the different liquids was also investigated with the results shown in Fig. 5(b). It can be seen that the amplitude of the received signals varies with different liquids contained, the higher the dielectric constant medium used for the senor, the smaller the amplitude of the received signal. This is because that the greater the dielectric constant, the less leakage current will flow through the substance, resulting in a higher voltage across the substance. The maximum amplitude, V_{PP}, of the oscillating signal at the receiver side is ~ 80 V for the clean water, and it is ~ 120 V for the 95% glycerin used, which is about 1.5 times that for the clean water case. The maximum amplitude of the oscillating signal at the receiver side becomes ~ 130 V when 75% ethanol is used as the liquid for sensing, which already approaches to the upper limit of coil transmission. It can be seen that the smaller the liquid dielectric constant ε_l, the greater the amplitude of the received signal. The FFT spectra of the received signals for different liquids with the liquid level of 40 cm are shown in Fig. 5(c). It can be clearly seen that the resonant frequency and amplitude of the signals for different solutions are different. This not only allows the real-time monitoring of liquid level, but also can be used to sense or distinguish different types of liquids for production line management.

2.6 Effects of C_{ID} on the sensor system

As shown by Eq. (3), the resonant frequency of the sensor system is dependent on the total capacitance of the sensor and the ID capacitor. The transmitter quality factor Q is also dependent on capacitance of the LC circuit, and is expressed as follows

$$Q = R\sqrt{\frac{C_S + C_{ID} + C_{TENG} + C_{par}}{L_1}} \quad (5)$$

According to this equation, the larger the fixed capacitance C_{ID} of the base capacitor, the higher the Q value of the transmitter. Higher Q value enables the sensor system to transmit the signal further and this was investigated to optimize the sensor system. Figure 6(a) is a comparison of the filtered signals of the receiver with C_{ID} = 30 and 100 pF, respectively, at a transmission distance of 20 cm and liquid height of 40 cm. Generally, lower frequency signal has smaller signal amplitude. The resonant frequency for the C_{ID} = 100 pF case is lower, and the maximum voltage V_{pp} in the time domain is similar to that for the C_{ID} = 30 pF case. The signal at the receiving end gradually weakens with the increase of the transmission distance as shown in Fig. 6(b). The signal amplitude for C_{ID} = 30 pF decays much faster than the case with C_{ID} = 100 pF. The received filtered signals with different C_{ID} are shown in Fig. 6(c) for a transmission distance = 100 cm. As it is clear that the maximum amplitude of the received signal has V_{pp} = ~ 750 mV for the C_{ID} = 100 pF case, whereas it is only about 225 mV for the C_{ID} = 30 pF case. At a long transmission distance, the sensor system with 100 pF C_{ID} can transmit signal much far away than the case with a 30 pF C_{ID}, because the former has a larger quality factor than the latter. The former is capable of transmitting signals up to 1.5 m yet with a relatively large amplitude of about V_{PP} ~ 60 mV with the details being included in SI4 in the ESM. The corresponding Q values are 154 and 112 respectively. It should be pointed out that 1.5 m is not the limit of the transmission distance of the sensor system as the signal amplitudes are still very large at the level of hundreds of millivoltages; but this transmission distance is normally good enough for most applications, therefore the maximum transmission distance is not investigated in detail in this work.

Figure 6(d) shows the amplitude of the resonant peak of the FFT spectra of the received signals with different C_{ID} as a function of transmission distance. Each point is the result of ten measurements, and the average values were taken for the plot. It can be clearly seen that for a fixed transmission distance, the FFT spectral amplitude of the resonant peak of the received signal for the large C_{ID} is much larger than those with small C_{ID}, it is about 10 dB difference for the whole transmission distances tested. Figure 6(e) shows the resonant frequency of the sensor system with different C_{ID} as a function of transmission distance with a fixed water level of 40 cm. For both the cases, the resonant

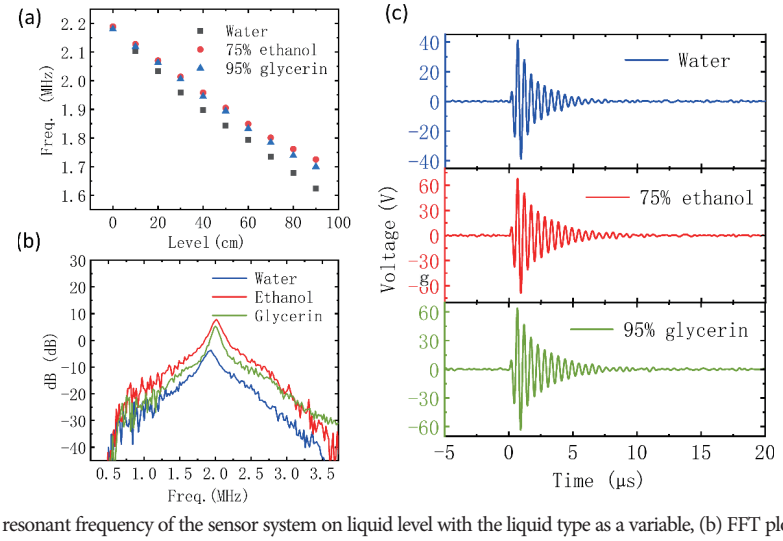

Figure 5 (a) Dependence of the resonant frequency of the sensor system on liquid level with the liquid type as a variable, (b) FFT plots for different liquids at the same level, frequency decreases as the dielectric constant rises, and (c) time domain waveforms for different liquids, the lower the dielectric constant, the higher the peak voltage V_{PP}.

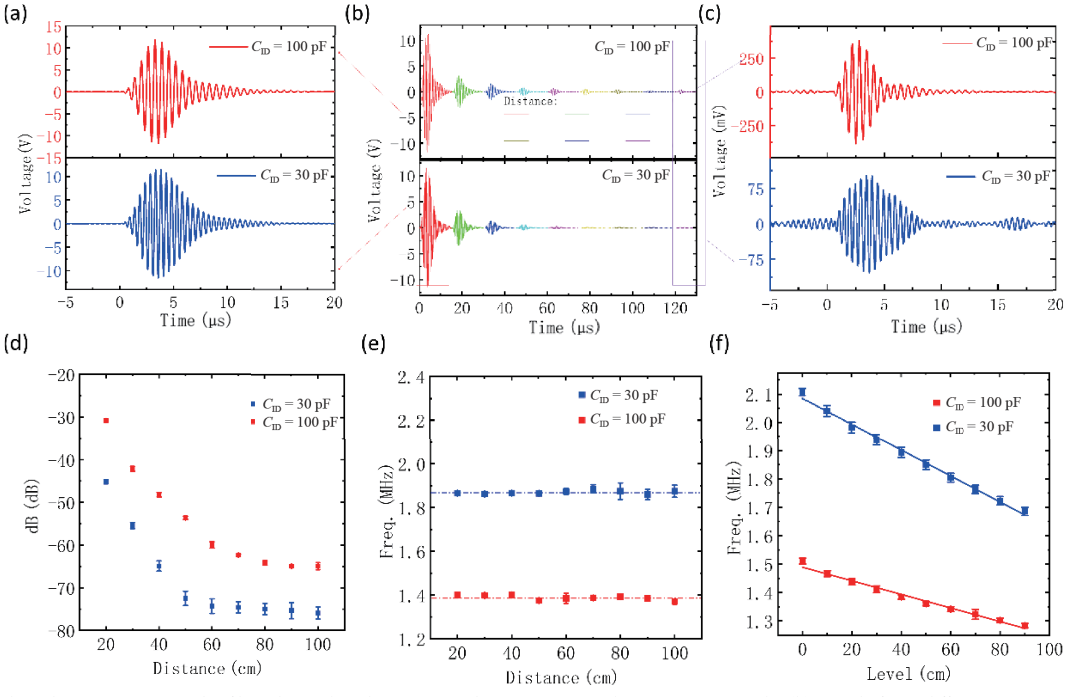

Figure 6 (a) When distance = 20 cm, the filtered signal at the receiver when C_{ID} is 30 and 100 pF respectively, (b) signals from different C_{ID} receivers at different distances, (c) when distance = 100 cm, the filtered signal at the receiver when C_{ID} is 30 and 100 pF respectively, (d) the amplitude of the desired peak of different C_{ID} signals after FFT at different distances, (e) the frequency of different C_{ID}s at different distances and (f) the frequency of receiver for different C_{ID} at different liquid level.

frequency remains almost unchanged, indicating that the transmission distance has little effect on resonant frequency of the sensor system.

Although higher Q value of the system can make the transmission distance longer, increasing C_{ID} also has some drawbacks. A large C_{ID} will reduce the sensitivity of the sensor system as normally the sensitivity of frequency-based sensors is proportional to f^a ($1 < a < 2$). According to Eq. (3), the larger the C_{ID}, the larger the variation range of frequency will be. Figure 6(f) shows dependence of the resonant frequency of the received signal on water level for different C_{ID}. For both the cases, the resonant frequency decreases linearly with the increase of liquid level, showing good linearity for the sensor. The frequency variation is from 2.11 to 1.70 MHz and from 1.51 to 1.28 MHz for C_{ID} having a value of 30 and 100 pF respectively. We define the sensitivity of the sensor as $s = \Delta f/\Delta h$, then the corresponding sensitivities are 4.626 and 2.273 kHz/cm, respectively, clearly showing that the smaller the C_{ID} makes the sensor system to have higher sensitivity. From the above analysis, it can be concluded that to design a high-performance wireless liquid level sensor system, a trade-off is needed for the transmission distance and sensitivity. Since the sensor has an excellent linearity, the transmission distance probably is far more important than the sensitivity. On the other hand, as shown in Fig. 6(c), the signal is clear and the maximum amplitude is in the range of ~ 100 mV. The modern electronics enables the development of circuit to handle much weaker signal, hence it is possible for further longer distance wireless transmission.

3 Conclusions

In this work, a TENG-based self-powered wireless and chipless sensor system has been proposed and demonstrated with a capacitive liquid level sensor. A high-performance TENG integrated with a synchronization microswitch for impedance match with the resonant circuit was fabricated and assessed using PA66 and FEP as the positive and negative triboelectric materials respectively. Using oxygen plasma to treat the surface of PA66 membrane can greatly improve the output capacity of TENG, and its maximum output voltage can reach 2,200 V. A liquid level sensor has been developed, which can respond to variation of liquid level well. The sensor system has a good linearity with the liquid level assessed with a gradient of 0.7 pF/cm. The TENG-based self-powered wireless liquid level sensor system has been designed and characterized. The sensor system showed fast and stable responses to liquid level variations with excellent repeatability. Furthermore, the factors that affect the transmitted signals have been analyzed and characterized in detail and methods to improve the wireless transmission distance and sensitivity have been proposed and investigated. The sensitivity and transmission distance of the sensing system can be achieved by optimizing the Q value of the circuit's quality factor, beneficiary for widespread application of this type of wireless sensor systems. This work has demonstrated the feasibility of the self-powered instantaneous wireless and chipless sensor system with excellent capability for applications.

4 Methods

4.1 Fabrication of TENG

The sensor system is shown in Fig. 1(a), which consists of a TENG, a magnetic resonance-coupled wireless transmission device, and a capacitive liquid level sensor. The TENG was fabricated using fluorinated ethylene propylene membrane as the negative triboelectric material and nylon-66 membrane as the positive triboelectric material. The FEP film with a thickness of 100 μm was purchased from Dupont. It was cut into a square of 5 cm × 5 cm and glued on the surface of a commercial acrylic support layer by a double-adhesive copper tape to form the negative tribo-plate. The PA66 membrane with a thickness of 100 μm was purchased from Dupont, and surface of the PA66 film was treated by oxygen plasma to increase the surface with higher positive surface potential, at a plasma power of 200 W for 2 min. Similarly, it was cut into a square of 5 cm × 5 cm and glued on the surface of an acrylic plate by a double-adhesive copper tape

to form the positive tribo-plate. They were then assembled together to form a TENG with a spacer of 4 mm using four springs.

4.2 Characterization instruments

A linear motor (H01-48 × 250) was utilized to control the cyclic contact force, frequency, and distance, which is able to control the force, contacting frequency, and traveling distance. The output voltages of the TENG were measured using an oscilloscope (Tektronix MDO3022). A Hitachi S3400N scanning electron microscope (SEM) was used to characterize the microstructure of the membranes. KPFM measurements were carried out using an atomic force microscope (AFM) system (Cypher-S, Asylum Research) with a Pt-coated Si probe.

Acknowledgements

This work was funded by National Key R&D Program of China (No. 2018YFB2002500), Zhejiang Province Key R & D programs (Nos. 2021C05004 and 2020C03039), NSFC (Nos. 61974037, 61904042, and 61801158), Natural Science Foundation of Zhejiang (No. LY21F040006), and Zhejiang University Education Foundation Global Partnership.

Electronic Supplementary Material: Supplementary material (enhancement of TENG performance with oxygen plasma treatment, SEM image and CPD value of tribo-membranes before and after oxygen plasma treatment, simulink-based system simulation circuit, theoretical analysis of liquid level sensor, performance of the sensing system at a 1.5 m transmission distance) is available in the online version of this article at https://doi.org/10.1007/s12274-022-4125-9.

References

[1] Wang, X. L.; Thompson, D. K.; Marshall, G. A.; Tymstra, C.; Carr, R.; Flannigan, M. D. Increasing frequency of extreme fire weather in Canada with climate change. *Clim. Change* **2015**, *130*, 573–586.

[2] Cai, W. J.; Borlace, S.; Lengaigne, M.; Van Rensch, P.; Collins, M.; Vecchi, G.; Timmermann, A.; Santoso, A.; McPhaden, M. J.; Wu, L. X. et al. Increasing frequency of extreme El Niño events due to greenhouse warming. *Nat. Clim. Change* **2014**, *4*, 111–116.

[3] Perera, A. T. D.; Nik, V. M.; Chen, D. L.; Scartezzini, J. L.; Hong, T. Z. Quantifying the impacts of climate change and extreme climate events on energy systems. *Nat. Energy* **2020**, *5*, 150–159.

[4] Midilli, A.; Dincer, I.; Ay, M. Green energy strategies for sustainable development. *Energy Pol.* **2006**, *34*, 3623–3633.

[5] Omer, A. M. Energy, environment and sustainable development. *Renewable Sustainable Energy Rev.* **2008**, *12*, 2265–2300.

[6] Sanchez Rodriguez, R.; Ürge-Vorsatz, D.; Barau, A. S. Sustainable development goals and climate change adaptation in cities. *Nat. Clim. Change* **2018**, *8*, 181–183.

[7] Van Aalst, M. K. The impacts of climate change on the risk of natural disasters. *Disasters* **2006**, *30*, 5–18.

[8] Tamari, S.; Mory, J.; Guerrero-Meza, V. Testing a near-infrared Lidar mounted with a large incidence angle to monitor the water level of turbid reservoirs. *ISPRS J. Photogramm. Remote Sens.* **2011**, *66*, S85–S91.

[9] Rosolem, J. B.; Dini, D. C.; Penze, R. S.; Floridia, C.; Leonardi, A. A.; Loichate, M. D.; Durelli, A. S. Fiber optic bending sensor for water level monitoring: Development and field test: A review. *IEEE Sens. J.* **2013**, *13*, 4113–4120.

[10] Grice, S.; Zhang, W.; Sugden, K.; Bennion, I. Liquid level sensor utilising a long period fiber grating. In *Proceedings of SPIE 7212, Optical Components and Materials VI*, San Jose, California, USA, 2009, 72120C.

[11] Kumar, B.; Rajita, G.; Mandal, N. A Review on capacitive-type sensor for measurement of height of liquid level. *Meas. Control* **2014**, *47*, 219–224.

[12] Radaideh, M. I.; Pigg, C.; Kozlowski, T.; Deng, Y. J.; Qu, A. N. Neural-based time series forecasting of loss of coolant accidents in nuclear power plants. *Exp. Syst. Appl.* **2020**, *160*, 113699.

[13] Aleksandrov, S. I.; Bol'shov, A. A.; Kornienko, A. V.; Novikov, I. V.; Postnikov, V. V.; Shishov, V. P.; Yurkin, G. V. Investigation of β-emission methods of monitoring coolant water level in nuclear power plants. *At. Energy* **2017**, *122*, 207–212.

[14] Zhu, L.; Alsaab, N.; Cheng, M. M. C.; Chen, P. Y. A zero-power ubiquitous wireless liquid-level sensor based on microfluidic-integrated microstrip Antenna. *IEEE J. Radio Frequ. Identificat.* **2020**, *4*, 265–274.

[15] Woodard, S. E.; Taylor, B. D. A wireless fluid-level measurement technique. *Sens. Actuators, A* **2007**, *137*, 268–278.

[16] Alreshaid, A. T.; Hester, J. G.; Su, W.; Fang, Y.; Tentzeris, M. M. Review-Ink-Jet printed wireless liquid and gas sensors for iot, smart Ag and smart city applications. *J. Electrochem. Soc.* **2018**, *165*, B407–B413.

[17] Loizou, K.; Koutroulis, E. Water level sensing: State of the art review and performance evaluation of a low-cost measurement system. *Measurement* **2016**, *89*, 204–214.

[18] Kim, J. Y.; Bae, S. E.; Park, T. H.; Paek, S.; Kim, T. J.; Lee, S. J. Wireless simultaneous measurement system for liquid level and density using dynamic bubbler technique: Application to KNO_3 molten salts. *J. Ind. Eng. Chem.* **2020**, *82*, 57–62.

[19] Kuang, K. S. C.; Quek, S. T.; Maalej, M. Remote flood monitoring system based on plastic optical fibres and wireless motes. *Sens. Actuators, A* **2008**, *147*, 449–455.

[20] Jin, J. X.; Wang, Y.; Jiang, H.; Chen, X. F. Evaluation of microclimatic detection by a wireless sensor network in forest ecosystems. *Sci. Rep.* **2018**, *8*, 16433.

[21] Lin, R. Z.; Kim, H. J.; Achavananthadith, S.; Kurt, S. A.; Tan, S. C. C.; Yao, H. C.; Tee, B. C. K.; Lee, J. K. W.; Ho, J. S. Wireless battery-free body sensor networks using near-field-enabled clothing. *Nat. Commun.* **2020**, *11*, 444.

[22] Fuh, Y. K.; Wang, B. S.; Tsai, C. Y. Self-powered pressure sensor with fully encapsulated 3D printed wavy substrate and highly-aligned piezoelectric fibers array. *Sci. Rep.* **2017**, *7*, 6759.

[23] Jin, L. M.; Tao, J.; Bao, R. R.; Sun, L.; Pan, C. F. Self-powered real-time movement monitoring sensor using triboelectric nanogenerator technology. *Sci. Rep.* **2017**, *7*, 10521.

[24] Sridhar, V.; Takahata, K. A hydrogel-based passive wireless sensor using a flex-circuit inductive transducer. *Sens. Actuators, A* **2009**, *155*, 58–65.

[25] Jang, S. D.; Kang, B. W.; Kim, J. Frequency selective surface based passive wireless sensor for structural health monitoring. *Smart Mater. Struct.* **2013**, *22*, 025002.

[26] Priya, S.; Ryu, J.; Park, C. S.; Oliver, J.; Choi, J. J.; Park, D. S. Piezoelectric and magnetoelectric thick films for fabricating power sources in wireless sensor nodes. *Sensors (Basel)* **2009**, *9*, 6362–6384.

[27] Li, P.; Wen, Y. M.; Liu, P. G.; Li, X. S.; Jia, C. B. A magnetoelectric energy harvester and management circuit for wireless sensor network. *Sens. Actuators, A* **2010**, *157*, 100–106.

[28] Vullers, R. J. M.; Schaijk, R. V.; Visser, H. J.; Penders, J.; Hoof, C. V. Energy harvesting for autonomous wireless sensor networks. *IEEE Solid-State Circuits Magaz.* **2010**, *2*, 29–38.

[29] Chen, C.; Wen, Z.; Shi, J. H.; Jian, X. H.; Li, P. Y.; Yeow, J. T. W.; Sun, X. H. Micro triboelectric ultrasonic device for acoustic energy transfer and signal communication. *Nat. Commun.* **2020**, *11*, 4143.

[30] Lei, H.; Xiao, J.; Chen, Y. F.; Jiang, J. W.; Xu, R. J.; Wen, Z.; Dong, B.; Sun, X. H. Bamboo-inspired self-powered triboelectric sensor for touch sensing and sitting posture monitoring. *Nano Energy* **2022**, *91*, 106670.

[31] Lei, H.; Chen, Y. F.; Gao, Z. Q.; Wen, Z.; Sun, X. H. Advances in self-powered triboelectric pressure sensors. *J. Mater. Chem. A* **2021**, *9*, 20100–20130.

[32] Zheng, Q.;Zhang, H.;Shi, B.;Xue, X.;Liu, Z.;Jin, Y.;Ma, Y.;Zou, Y.;Wang, X.;An, Z. et al. In vivo self-powered wireless cardiac

monitoring via implantable triboelectric nanogenerator. *ACS Nano* **2016**, *10*, 6510–6518.

[33] Lu, H. W.; Shi, H. J.; Chen, G. R.; Wu, Y. H.; Zhang, J. W.; Yang, L. Y.; Zhang, Y. J.; Zheng, H. W. High-performance flexible piezoelectric nanogenerator based on specific 3D nano BCZT@Ag hetero-structure design for the application of self-powered wireless sensor system. *Small* **2021**, *17*, 2101333.

[34] Han, M. D.; Zhang, X. S.; Sun, X. M.; Meng, B.; Liu, W.; Zhang, H. X. Magnetic-assisted triboelectric nanogenerators as self-powered visualized omnidirectional tilt sensing system. *Sci. Rep.* **2014**, *4*, 4811.

[35] Zhao, X. J.; Wei, G. W.; Li, X. H.; Qin, Y.; Xu, D. D.; Tang, W.; Yin, H. J.; Wei, X. K.; Jia, L. M. Self-powered triboelectric nano vibration accelerometer based wireless sensor system for railway state health monitoring. *Nano Energy* **2017**, *34*, 549–555.

[36] Xie, X. K.; Chen, Y. F.; Jiang, J. X.; Li, J. Y.; Yang, Y. Q.; Liu, Y. N.; Yang, L.; Tu, X.; Sun, X. H.; Zhao, C. et al. Self-powered gyroscope angle sensor based on resistive matching effect of triboelectric nanogenerator. *Adv. Mater. Technol.* **2021**, *6*, 2100797.

[37] Zhang, T. T.; Wen, Z.; Lei, H.; Gao, Z. Q.; Chen, Y. F.; Zhang, Y.; Liu, J. Y.; Xie, Y. L.; Sun, X. H. Surface-microengineering for high-performance triboelectric tactile sensor via dynamically assembled ferrofluid template. *Nano Energy* **2021**, *87*, 106215.

[38] Yin, W. L.; Xie, Y. D.; Long, J.; Zhao, P. F.; Chen, J. K.; Luo, J. K.; Wang, X. Z.; Dong, S. R. A self-power-transmission and non-contact-reception keyboard based on a novel resonant triboelectric nanogenerator (R-TENG). *Nano Energy* **2018**, *50*, 16–24.

[39] Chen, J. K.; Xuan, W. P.; Zhao, P. F.; Farooq, U.; Ding, P.; Yin, W. L.; Jin, H.; Wang, X. Z.; Fu, Y. Q.; Dong, S. R. et al. Triboelectric effect based instantaneous self-powered wireless sensing with self-determined identity. *Nano Energy* **2018**, *51*, 1–9.

[40] Zhang, C.; Chen, J. K.; Xuan, W. P.; Huang, S. Y.; You, B.; Li, W. J.; Sun, L. L.; Jin, H.; Wang, X. Z.; Dong, S. R. et al. Conjunction of triboelectric nanogenerator with induction coils as wireless power sources and self-powered wireless sensors. *Nat. Commun.* **2020**, *11*, 58.

[41] Tang, Y. Z.; Xuan, W. P.; Zhang, C.; Xu, L. Q.; Liu, F. H.; Chen, J. K.; Jin, H.; Ye, Z.; Cao, Z.; Li, Y. B. et al. Fully self-powered instantaneous wireless traffic monitoring system based on triboelectric nanogenerator and magnetic resonance coupling. *Nano Energy* **2021**, *89*, 106429.

[42] Xu, L. Q.; Xuan, W. P.; Chen, J. K.; Zhang, C.; Tang, Y. Z.; Huang, X. W.; Li, W. J.; Jin, H.; Dong, S. R.; Yin, W. L. et al. Fully self-powered instantaneous wireless humidity sensing system based on triboelectric nanogenerator. *Nano Energy* **2021**, *83*, 105814.

[43] Chen, Y. D.; Jie, Y.; Zhu, J. Q.; Lu, Q. X.; Cheng, Y.; Cao, X.; Wang, Z. L. Hybridized triboelectric-electromagnetic nanogenerators and solar cell for energy harvesting and wireless power transmission. *Nano Res*, in press, https://doi.org/10.1007/s12274-021-3822-0.

[44] Zhang, C.; Chen, J. K.; Xuan, W. P.; Huang, S. Y.; Shi, L.; Cao, Z.; Ye, Z.; Li, Y. B.; Wang, X. Z.; Dong, S. R. et al. Triboelectric nanogenerator-enabled fully self-powered instantaneous wireless sensor systems. *Nano Energy* **2021**, *92*, 106770.

[45] Wen, F.; Wang, H.; He, T. Y. Y.; Shi, Q. F.; Sun, Z. D.; Zhu, M. L.; Zhang, Z. X.; Cao, Z. G.; Dai, Y. B.; Zhang, T. et al. Battery-free short-range self-powered wireless sensor network (SS-WSN) using TENG based direct sensory transmission (TDST) mechanism. *Nano Energy* **2020**, *67*, 104266.

[46] Niu, S. M.; Wang, S. H.; Lin, L.; Liu, Y.; Zhou, Y. S.; Hu, Y. F.; Wang, Z. L. Theoretical study of contact-mode triboelectric nanogenerators as an effective power source. *Energy Environ. Sci.* **2013**, *6*, 3576–3583.

[47] Zhang, X. S.; Han, M. D.; Wang, R. X.; Meng, B.; Zhu, F. Y.; Sun, X. M.; Hu, W.; Wang, W.; Li, Z. H.; Zhang, H. X. High-performance triboelectric nanogenerator with enhanced energy density based on single-step fluorocarbon plasma treatment. *Nano Energy* **2014**, *4*, 123–131.

[48] Chen, J.; Yang, J.; Li, Z. L.; Fan, X.; Zi, Y. L.; Jing, Q. S.; Guo, H. Y.; Wen, Z.; Pradel, K. C.; Niu, S. M. et al. Networks of triboelectric nanogenerators for harvesting water wave energy: A potential approach toward blue energy. *ACS Nano* **2015**, *9*, 3324–3331.

[49] Rodrigues, C.; Nunes, D.; Clemente, D.; Mathias, N.; Correia, J. M.; Rosa-Santos, P.; Taveira-Pinto, F.; Morais, T.; Pereira, A.; Ventura, J. Emerging triboelectric nanogenerators for ocean wave energy harvesting: State of the art and future perspectives. *Energy Environ. Sci.* **2020**, *13*, 2657–2683.

[50] Chen, B.; Yang, Y.; Wang, Z. L. Scavenging wind energy by triboelectric nanogenerators. *Adv. Energy Mater.* **2018**, *8*, 1702649.